Transport analysis and modelling of the evolution of hollow density profiles plasmas in JET and implication for ITER

2015 Nucl. Fusion 55 123001

(http://iopscience.iop.org/0029-5515/55/12/123001)

IOP Publishing | International Atomic Energy Agency Nuclear Fusion

Nucl. Fusion **55** (2015) 123001 (18pp) doi:10.1088/0029-5515/55/12/123001

Transport analysis and modelling of the evolution of hollow density profiles plasmas in JET and implication for ITER

B. Baiocchi[1], C. Bourdelle[1], C. Angioni[2], F. Imbeaux[1], A. Loarte[3] M. Maslov[4] and JET Contributors[5]

EUROfusion Consortium, JET, Culham Science Centre, Abingdon, OX14 3DB, UK
[1] CEA, IRFM, F-13108 St. Paul-lez-Durance, France
[2] Max-Planck-Institut für Plasmaphysik, 85748 Garching, Germany
[3] ITER Organization, Route de Vinon-sur-Verdon, CS 90 046, 13067 St Paul Lez Durance Cedex, France
[4] CCFE, Culham Science Centre, Abingdon, OX14 3DB, UK

E-mail: baiocchi@ifp.cnr.it

Received 22 December 2014, revised 3 August 2015
Accepted for publication 14 August 2015
Published 15 October 2015

Abstract

The density evolution during the transient phase just after the L–H transition is investigated using theoretical transport models. Cases characterized by core densities which evolve in longer timescales than the edge densities, leading to hollow density profiles ($R/L_n = -R\nabla n/n < 0$) are modelled. This density evolution is particularly interesting because it has been shown to be beneficial in the view of the access to burning plasma conditions in ITER (Loarte *et al* 2013 *Nucl. Fusion* **53** 083031). Self-consistent simulations of the JET discharge 79676 of the density-only, and of the density and the temperatures are carried out using a quasilinear gyrokinetic code, QuaLiKiz (Bourdelle *et al* 2007 *Phys. Plasmas* **14** 112501), coupled with a transport code CRONOS (Artaud *et al* 2010 *Nucl. Fusion* **50** 043001). The slow evolution of the hollow density, associated with the self-consistently calculated hollow NBI particle deposition, is well reproduced in the plasma core. Indeed, QuaLiKiz is shown to reproduce nonlinear gyrokinetic heat and particle fluxes well for both positive and negative R/L_n. That gives a theoretical and general basis for the persistence of the hollowness, laying the groundwork for the extrapolation to ITER.

Keywords: tokamak, transport, modelling

(Some figures may appear in colour only in the online journal)

1. Introduction

To understand and predict particle transport in present and future fusion machines is essential in order to achieve a large amount of fusion power. Indeed, the L–H power threshold scales almost linearly up with density [1] and the fusion power scales with the square of the density of the plasma.

The mechanisms underlying the particle transport in the plasma core have been extensively investigated both through experimental works and theoretical studies. Recently, progress in describing the particle transport due to turbulence has been made, achieving good agreement between theoretical expectations and experimental observations at a given time of the analysed pulses [2, 3]. However, time evolution of density profiles has not yet been extensively modelled. In particular, some particle transport phenomena still require a deep investigation, as the evolution of the plasma density just after the confinement transitions (for example L–H or H–L). This issue can have important consequences on the confinement state of the plasma and on the performances of the future fusion machines as discussed in [4].

The work presented in this paper starts from the experimental analysis carried out in [4], where the build-up of

[5] See the appendix of [42].

plasma density and temperature following the H-mode transition has been studied. JET low collisionality pulses are particularly studied and perspectives for ITER are drawn. In the JET pulses, while the timescales of the build-up of both the core and the edge temperatures are found to be comparable to the energy confinement time, τ_E, the core density evolves in timescales much longer than the ones characteristic for the edge density. This evolution was found in the case of JET discharges with high plasma current and coexistent hollow NBI particle deposition profile. They are the closest point to ITER in the operation space considering all dimensionless parameters [5]. Contrarily to the stationary phase, where a high core density is directly connected to a high fusion power, a slow increase of the core density with respect to the core temperature right after the L–H transition is expected to be beneficial in ITER. As illustrated in [4], this evolution leads indeed to a reduced radiation power, in addition to a large alpha power given by the growth of the temperature, assuring the level of power required to sustain the H-mode confinement.

This observed slow core density evolution gives encouraging indications for accessing burning plasma conditions and sustaining ITER baseline regime. It is therefore essential to understand and model such JET pulses to allow more confident ITER scenario predictions. So far, simulations of these JET discharges based on the empirical turbulent transport model called 'Bohm–gyroBohm' [6] have been carried out. The experimental profiles evolution has been reproduced assuming a pure diffusive particle transport, with a lower diffusion coefficient (of about ¼–½) than the values used to model density profiles of stationary JET discharges [7]. However, in view of physics-based extrapolations for ITER, the physics mechanisms which lead to the slow evolution of the hollow density profiles remain to be studied, and a complete physics-based modelling of the transient phase of the JET H-modes characterized by this behaviour is needed.

In this context, the theory-based gyrokinetic quasilinear transport model QuaLiKiz [8] is used to investigate the physics mechanisms at play in presence of a hollow density profile ($R/L_n < 0$, where $R/L_n := -R\nabla n/n$) as well as modelling self-consistently the JET discharges core evolution thanks to the coupling in the transport code CRONOS [9]. In this work, the carbon wall baseline JET discharge 79676 has been studied and simulated. This pulse is a typical example of ITER relevant high current JET H-mode characterized by a slow relaxation of the hollow density profile during the transient phase after the L–H transition.

First, the validity of the model has been checked in the negative R/L_n domain through a benchmark with the gyrokinetic code GKW [10] run in both its quasilinear and nonlinear versions. The stand-alone analysis of the growth rates and the particle fluxes as a function of R/L_n has been carried out. The agreement between the two codes legitimizes the use of the faster QuaLiKiz to deepen the stand-alone study and to carry out the self-consistent modelling inside CRONOS. Parametric scans of key parameters such as the collisionality, the values of the ion and electron temperature gradient lengths (respectively R/L_{Ti} and R/L_{Te}) and their ratio (L_{Ti}/L_{Te}) are then carried out for $R/L_n < 0$. Some general trends are deduced, and compared with the case $R/L_n > 0$. They are used as theoretical basis in order to understand the behaviour of the density evolution of the investigated JET discharge, in view of prediction of ITER plasmas.

Finally, self-consistent simulations of the transient phase following the H-mode transition are carried out, modelling the density-only and the density together with the temperatures for the JET discharge 79676. The NBI heat and particle sources are self-consistently modelled using the Monte Carlo NEMO/SPOT codes [11]. The resulting weak turbulent fluxes are consistent with the slow density profile evolution which is mostly due to the weak core particle source.

In section 2, the profiles and the time evolution of the parameters that characterize the analysed experimental JET carbon wall H-mode discharge are described, and the ITER relevance of this discharge is highlighted. Section 3 presents the results of the benchmark between QuaLiKiz and GKW and summarizes the trends of the parametric scans, which are more extensively described in the appendix. In section 4, the self-consistent modelling of the JET H-mode discharge after the H-mode transition carried out with QuaLiKiz in the integrated transport code CRONOS, using NEMO/SPOT for the NBI modelling, is presented. The summary and some conclusions follow in section 5.

2. Experimental data

The analysed JET discharge 79676 is a high plasma current H-mode shot, characterized by $I_p = 4.3$ MA, $B_T = 3.4$ T, $P_{NBI} = 21$ MW and a high level of gas puffing (gas fuelling rate ~3.5×10^{22} s^{-1}). Because of the high plasma current, both the plasma density and the plasma temperature are large, leading to relatively low core collisionality. The NBI particle deposition profile becomes hollow after the H-mode transition, as it is shown in figure 1(*a*). A low collisionality and an off axis particle source are both as close as presently possible to an ITER relevant case (the discharge 79676 is characterized by a $\nu^*_{vol.avg} \sim 0.005$, and the typical expected ITER reference scenario $\nu^*_{vol.avg} \sim 0.002$, where $\nu^* := \nu_{ie}/\varepsilon^{2/3}/(c_{the}qR)$, $\varepsilon = r/R$, $c_{the} = \sqrt{2T_e/m_e}$, [5]). The density evolution in such a plasma is therefore of high interest in view of ITER operation. As reported in the analysis carried out in [4] and here illustrated by figure 1(*b*), the core density evolves more slowly than the edge density. The edge density builds up at a time of the order of the energy confinement time, τ_E ($\tau_E \sim 0.4$ s). This leads to a density profile, entirely hollow up to $1\tau_E$ after the L–H transition, which becomes completely relaxed only after a sawtooth event (occurring after ~$3\tau_E$). On the contrary, the whole profiles of the ion and electron temperatures react both in a stiff way to the L–H transition, evolving to the stationary state in ~$1\tau_E$, keeping T_e/T_i close to 1 during all the investigated evolution time (figure 2).

The time of the complete pedestal build up ($1\tau_E$ after the L–H transition, i.e. $t = 9.8$ s) has been chosen as the initial point for the self-consistent time evolving simulations of this work. Figure 3(a) shows the experimental profile of the density at that time, together with the fit of the data used as input of the simulation. The whole profile has a positive

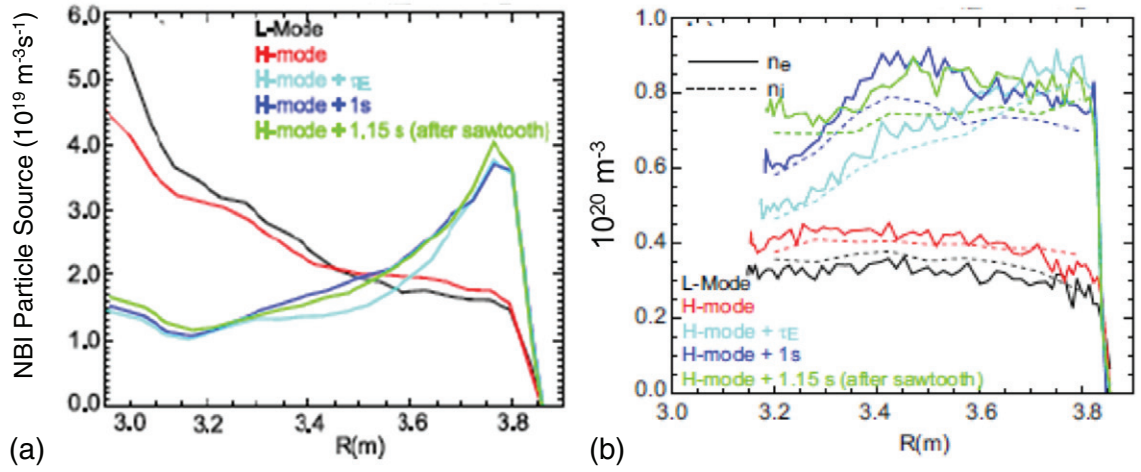

Figure 1. (*a*) NBI particle deposition and (*b*) density profiles during the evolution of the discharge 79676 (taken from [3]).

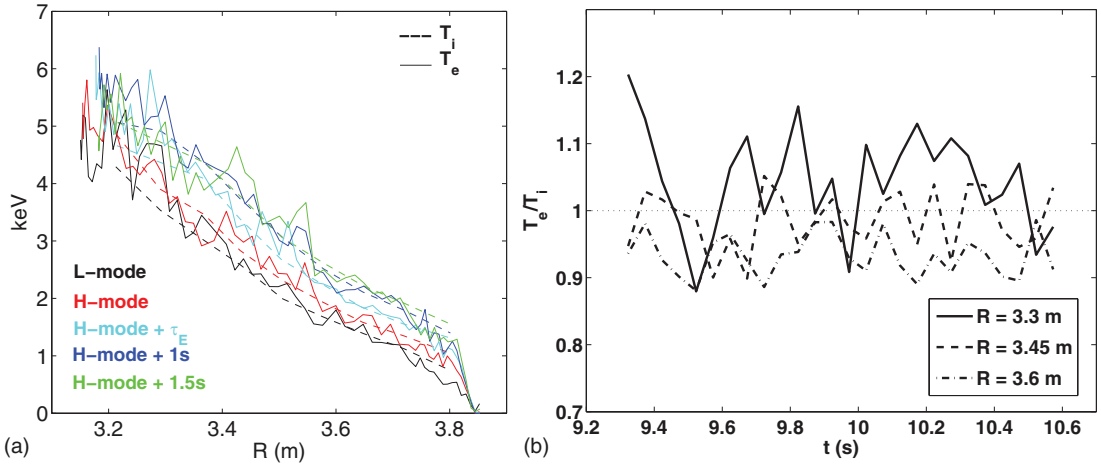

Figure 2. (*a*) Electron (full lines) and ion (dashed lines) temperature profiles during the evolution of the JET discharge 79676. (*b*) T_e/T_i ratio versus time at three radii.

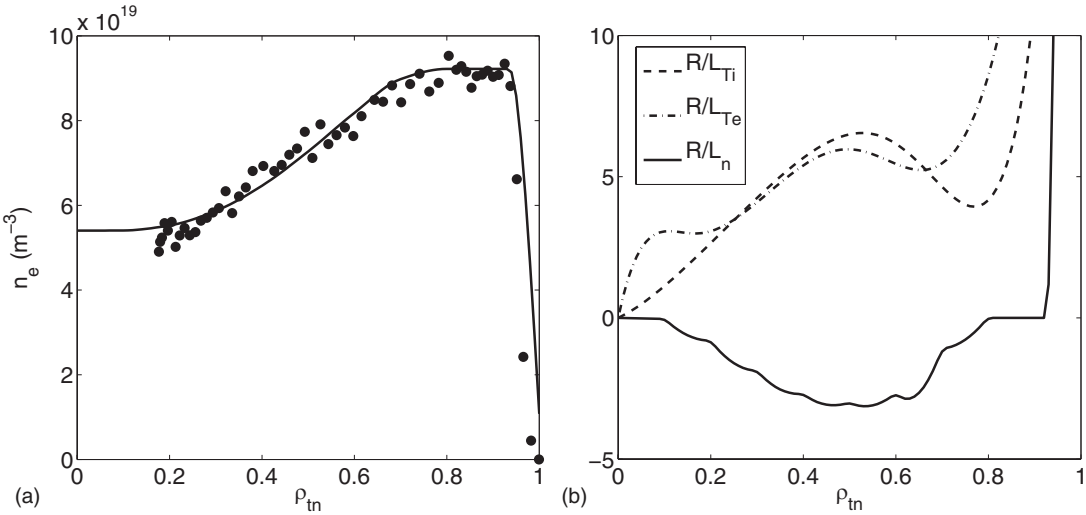

Figure 3. (*a*) Density and (*b*) R/L_{ne}, $R/L_{Ti,e}$ profiles as a function of the normalized toroidal flux coordinate ρ_{tn}. Data taken from the experimental database of the JET discharge 79676 at 9.8 s.

gradient, except at the edge, where the density is flat or has a strongly negative gradient as expected in the pedestal region. In figure 3(*b*), the R/L_{ne} and R/L_T profiles are shown. A negative value of R/L_{ne} means a positive gradient of density, i.e. a hollow density profile. As one can see from figure 3(*b*), $R/L_T \sim 6$ at mid-radius, which is regularly observed in present H-mode plasmas and which is in the range of values which are expected for the ITER baseline scenario.

3. QuaLiKiz stand-alone analysis of negative R/L_n plasmas: benchmark with GKW and parametric studies

Extensive theoretical and experimental studies have been carried out in order to investigate and predict positive R/L_n. Following recent comprehensive analyses [3, 12, 13], the behaviour of the density peaking can be regarded as the macroscopic expression of the turbulent state of the plasma, (i.e. the nature of the modes and their frequency), which is governed by a complex combination of several physical parameters and of the direct influence of the external sources. Most of the parametric dependences can be explained and predicted by a quasilinear approach, in terms of particle convection mechanisms, and are widely experimentally confirmed [3].

For negative R/L_n no such deep investigation has been carried out. In a very recent study about pellet fuelled discharges of MAST [14], the transport properties of the hollow density, transiently driven by pellet injection, have been investigated. This first microstability analysis predicts the stabilization of the modes for negative R/L_n, giving significant indications about the behaviour of the plasma in presence of hollow density profiles. However these results refer to a specific plasma configuration far from JET plasmas. In addition, the results have been found highly dependent on the rapid and large transient changes of several physical parameters. Additional investigations are then mandatory in order to find general results and to individuate the validity interval of these recent findings.

The strong physics basis obtained from the studies for positive R/L_n ensures general validity of the gyrokinetic models, and allows to enlarge the analysis to the cases with $R/L_n < 0$. For this reason, the results of complete and first principle gyrokinetic codes like GKW are considered reliable for both positive and negative R/L_n. Then, to validate the quasilinear reduced gyrokinetic transport model QuaLiKiz at negative R/L_n, a benchmark with GKW is carried out. QuaLiKiz is then used to investigate the dependences of the particle flux convective and diffusive contributions with respect to plasma parameters which are known to be relevant to turbulent particle transport.

3.1. Benchmark among the gyrokinetic transport models

In order to investigate the mechanisms at the basis of particle transport for $R/L_n < 0$, the quasi linear gyrokinetic code QuaLiKiz and the more complete gyrokinetic code GKW have been used in a preliminary parametric study of the quantity R/L_n. The particle fluxes and the growth rate spectra obtained by the two codes by varying R/L_n have been analysed. The set of values used in the study, characterized by high density, high temperature and low collisionality, is reported in table 1. They are taken at mid-radius and in the range of the values expected for the ITER baseline scenario, except for R/L_T, which is foreseen to be lower (rather $R/L_T = 6$). Here a larger R/L_T of 9, leading to a case further above the critical temperature threshold, has been chosen. This allows to speed up the convergence to saturated states in the nonlinear simulations of GKW for the cases with $R/L_n < 0$, which are linearly less unstable. The goal of this first study is indeed to benchmark QuaLiKiz with GKW in the quasi-linear framework and to compare the obtained fluxes with nonlinear GKW fluxes.

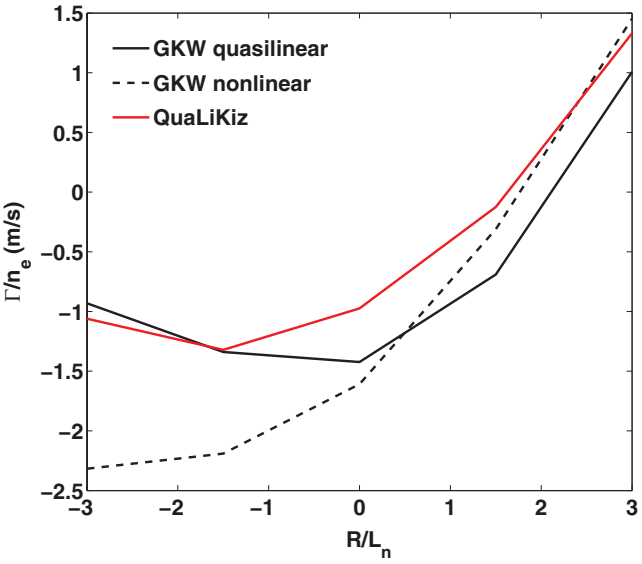

Figure 4. Particle flux divided by the density as a function of R/L_n, calculated by the gyrokinetic codes QuaLiKiz and GKW.

Table 1. Values of the parameters used as input for a parametric scan in R/L_n. n_e is the electron density, T_e (T_i) is the electron (ion) temperature, q is the safety factor, s is the magnetic shear, ρ_{tn} is the normalized toroidal flux coordinate, Z_{eff} is the plasma effective charge, α is the normalized plasma pressure gradient.

Parameters	Values
$R/L_n = R/L_{ne} = R/L_{ni}$	$-3, -1.5, 0, 1.5, 3$
n_e	1e20 m^{-3}
$R/L_T = R/L_{Te} = R/L_{Ti}$	9
$T_e = T_i$	9 keV
q	1.2
s	0.58
ρ_{tn}	0.5
Z_{eff}	1.7 (carbon/deuterium)
α	0
Collisions	Yes ($\nu^* = 0.0118$)

In figure 4, the total particle fluxes are shown as a function of R/L_n. A good agreement between quasilinear fluxes produced by QuaLiKiz and GKW has been found for both positive and negative R/L_n. For $R/L_n < 0$, the particle flux is always directed inward. It is maximum for values of R/L_n close to 0, and it tends to decrease for higher negative R/L_n. For $R/L_n > 0$, the flux passes from being inward to outward, increasing with increasing R/L_n.

For negative R/L_n, a discrepancy between quasilinear and nonlinear particle GKW fluxes has been found, as illustrated by figure 4. The saturation amplitude in all the quasilinear GKW transport channels has been set by matching the quasi linear and the nonlinear ion heat flux for the case at $R/L_n = 0$. A calibration factor is always needed to obtain quasilinear fluxes, because of the systematic quasilinear overestimation of the flux weights with respect to the nonlinear

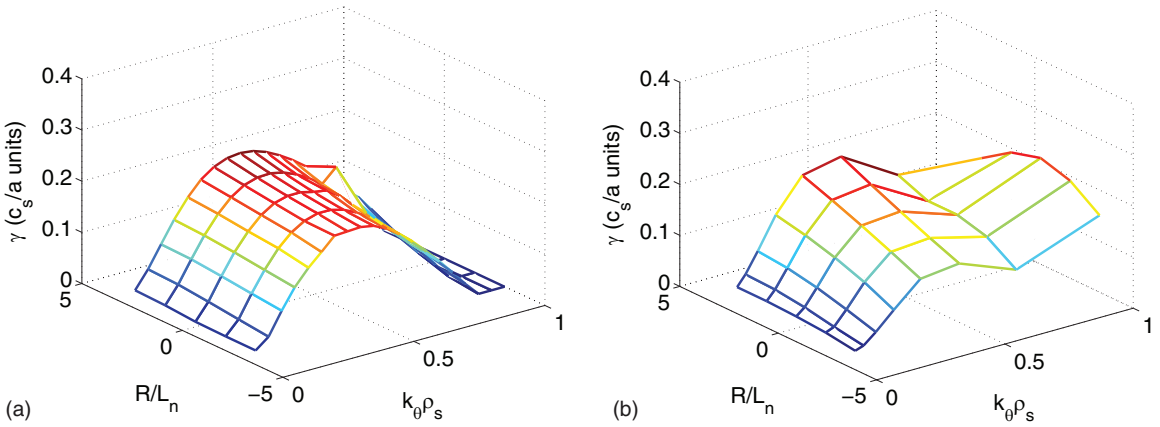

Figure 5. Normalized growth rates as functions of $k_\theta\rho_s$ and of R/L_n, obtained by QuaLiKiz (a) and the quasi-linear GKW (b). c_s is the sound velocity, defined above, a is the minor radius.

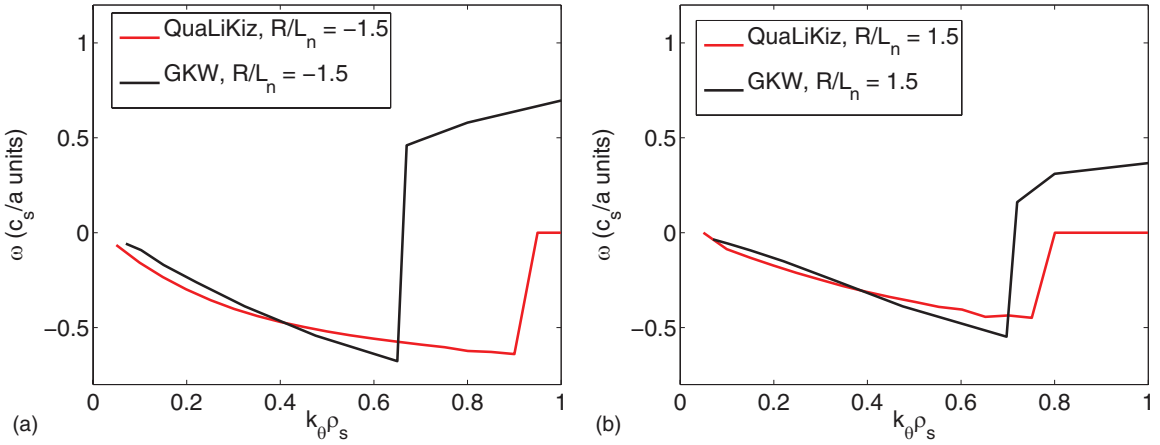

Figure 6. Normalized frequencies relative to the growth rates of figure 5 as functions of $k_\theta\rho_s$ for $R/L_n = -1.5$ (a) and $R/L_n = 1.5$ (b), obtained by QuaLiKiz and the quasi-linear GKW. Negative (positive) values mean ion (electron) drift direction. c_s is the sound velocity, defined above, a is the minor radius.

flux weights [15–17]. The discrepancy at negative values of R/L_n between the quasilinear and the nonlinear results can be therefore connected to a different ratio between the quasilinear and the nonlinear fluxes of particle and ion heat. Following previous studies [15, 18, 19], the investigation of the origin of this difference has been carried out by computing the quasilinear fluxes as spectral averages of the quasilinear phase shifts and amplitudes over the actual spectrum of the nonlinear electrostatic potential. It has revealed that the discrepancy between nonlinear and quasilinear results is largely produced by a difference between the quasilinear and the nonlinear phase shifts of the ion heat flux, rather than between those of the particle flux, which, in contrast, are much closer, also at negative values of R/L_n. A deeper and more comprehensive investigation of these differences will be the subject of future research. However, one must keep in mind that these differences might be at least partly responsible of the discrepancies between the predicted and the measured profiles which are found when density only and combined density and temperature simulations are performed with QuaLiKiz in CRONOS, as reported in section 4.

Focusing on the quasilinear fluxes, the QuaLiKiz growth rate spectra are compared to GKW's (see figure 5). For normalized poloidal wave numbers such that $k_\theta\rho_s < 0.6$ (ρ_s is defined as $c_s/(eB/m_i c)$, where $c_s = \sqrt{T_e/m_i}$, e is the electron charge, B the magnetic field, m_i the ion mass, T_e the electron temperature), the growth rates, for both models, similarly slightly decrease with decreasing R/L_n. The agreement is good also for the frequencies, as shown in figure 6 where the cases such that $R/L_n = \mp\ 1.5$ are illustrated. Negative frequencies mean that the mode is drifting in the ion diamagnetic direction, such modes are commonly named ion temperature gradient modes (ITG). Positive frequencies mean that the mode is drifting in the electron diamagnetic direction, such modes are commonly named trapped electron modes (TEM). The most unstable modes for $k_\theta\rho_s < 0.6$ are always in the ion drift direction (ITG dominated), for both positive and negative R/L_n. While for $R/L_n > 0$, QuaLiKiz has been already widely benchmarked for a large interval of $k_\theta\rho_s$, for $R/L_n < 0$ an extensive work of benchmarking has not been carried out. For high $k_\theta\rho_s$, some discrepancy between the models is reported. However in ITG dominated regimes, the maximum growth

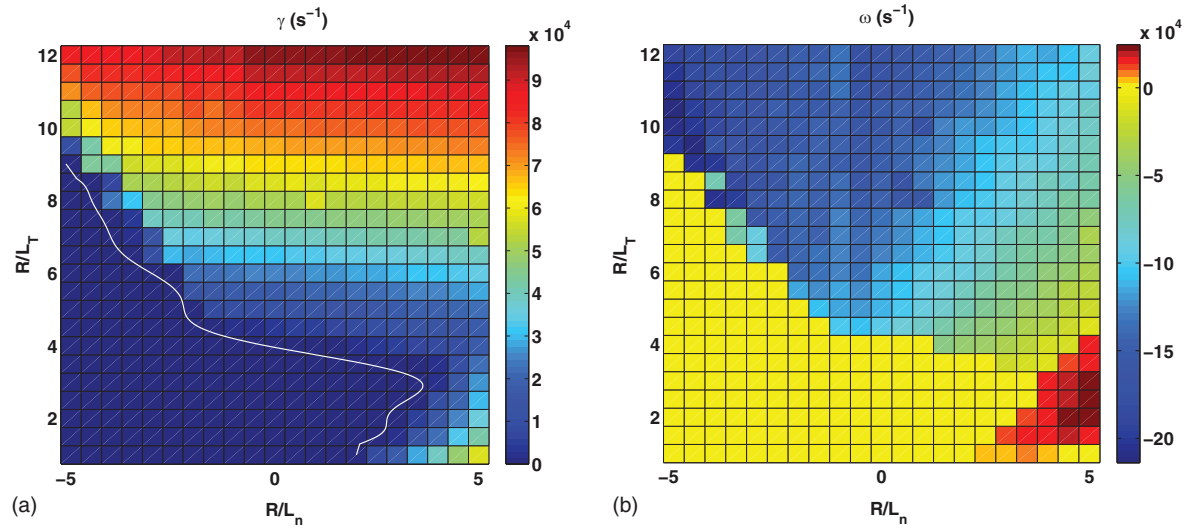

Figure 7. Growth rates (*a*) and relative frequencies (*b*) as functions of R/L_T and R/L_n, obtained by QuaLiKiz. Apart from $R/L_{Ti} = R/L_{Te} = R/L_T$, which are taken in the interval [1, 12] and R/L_n, which is extended to [−5 5], the input parameters values of this parametric scan are reported in table 1. The white line in (a) represents the spline interpolation of the $\gamma = 0$ boundary.

rate is usually found for $k_\theta\rho_s \approx 0.3$, and low $k_\theta\rho_s$ instabilities are known to give the main contribution to the turbulent particle flux. Then, since the theory predicts the full stabilization of TEM for $R/L_n < 0$, the discrepancy at higher $k_\theta\rho_s$ does not have any relevant consequence for the prediction of the turbulent particle transport in presence of hollow density profiles.

In the rest of this section, the impact of a hollow density profile is described by the faster model QuaLiKiz in good agreement with the more complete gyrokinetic code GKW (used in its quasi-linear version). In particular, a parametric investigation of the particle flux is carried out.

3.2. Parametric scans and dependences

The agreement between the quasilinear particle fluxes produced by QuaLiKiz and GKW justifies the use of QuaLiKiz to enlarge the analysis of the instabilities in presence of R/L_n from −5 to 5. The impact of R/L_T is extended from 1 to 12, i.e. including lower values more relevant to the foreseen ITER baseline scenario.

In figure 7, the maximal growth rates for $k_\theta\rho_s < 1$ and the corresponding frequencies are shown as functions of R/L_n and R/L_T. The figure shows the domain where ion (respectively electron) drifting modes dominate, called the ITG (respectively TEM) domain. In agreement with the theoretical expectations [20], the ITG dominated instabilities are present over a certain critical value of R/L_T. For negative R/L_n this temperature gradient threshold is higher for higher absolute values of R/L_n. For positive R/L_n, for the dominant ITG mode, higher absolute value of the frequency corresponds to lower R/L_n [12, 13]. TEM dominated instabilities raise only at large and positive values of R/L_n, in agreement with [14]. They are destabilized by large and positive R/L_n, reinforcing the asymmetry observed in figure 7.

To identify the main mechanisms of particle transport due to the instabilities the general following expression of the electron flux (in $m^{-2}\ s^{-1}$) is used [3]:

$$\Gamma = \frac{n_e}{R}\left(-D\frac{R}{L_{ne}} + RV_{th} + RV_c\right). \quad (1)$$

Here n_e is the electron density, R is the major radius. The first term inside the parenthesis is the diffusive contribution, given by the diffusivity coefficient D and the normalized relative density gradient $R/L_{ne} = -R\nabla n_e/n_e$. The second and the third terms represent the convection contributions: the thermodiffusivity RV_{th}, which depends on the electron temperature gradient such that $V_{th} = -C_{th}R\nabla T_e/T_e$, and the compressibility or pure convection term RV_c. A positive flux or convective velocity means that the transport is directed outward. Here the impact of rotation is not included. Indeed, the roto-diffusion term is negligible on electrons due to their small mass [21].

The behaviour of the convective terms has been found in the experiments to be influenced by several physics parameters [3, 13]. As reported in detail in the appendix and here below summarized, QuaLiKiz is used to isolate the compressibility and the thermodiffusion convective terms in different regimes. The analysis is focused on negative values of R/L_n, while including for comparison the previously well investigated positive R/L_n domain [3, 12, 13, 22]. We start the analysis by choosing $R/L_{Ti} = R/L_{Te} = 6$, value in the range expected for the ITER baseline scenario, and we study the variation of the flux contributions varying the collisionality, R/L_T and the ratio $R/L_{Ti}/R/L_{Te}$. The following trends have been found (for more details and illustrations see the appendix):

(1) Concerning the impact of collisionality, for negative R/L_n and for R/L_T of 6, the total convection is low and outward (the outward compressibility being of the same order as the inward thermodiffusion). It leads to a weak total flux, which is inward over collisionalities ranging from 0 to values typical of real experiments. For $R/L_n > 0$, the known result of having an inward flux in the collisionless limit switching to an outward flux for finite and low ν^* is recovered [23]. Ultimately, for positive higher R/L_n, the

flux is outward even in the collisionless regime, with a dominant positive thermodiffusion for almost all ν^*.

(2) With an increasing $R/L_T = R/L_{Ti} = R/L_{Te}$, all the flux contributions are enlarged as expected. In the case of negative R/L_n, the total convection becomes inward because of the dominance of the thermodiffusion. The total flux amplitude is then larger and remains directed inward up to high values of ν^* ($\nu^* \sim 0.1$). For positive R/L_n, the sign inversion takes place always for very low values of collisionality, leading to a stronger outward total flux for finite ν^*.

(3) Increasing R/L_{Ti} at fixed R/L_{Te} gives a similar though weaker trend due to a weaker increase of the thermodiffusion.

(4) Increasing R/L_{Te} at fixed R/L_{Ti} leads to enlarged thermodiffusion. The total flux is then directed more inward. For negative R/L_n it means stronger inward fluxes for ν^* up to rather large values ($\nu^* \sim 0.08$).

Overall, with negative R/L_n, the total convection is weaker than with positive R/L_n, hence leading to weakly evolving hollow density profiles, as observed in the JET discharge presented in section 2. This behaviour is even stronger when decreasing R/L_{Te} or/and R/L_{Ti}, while the evolution becomes faster for higher R/L_{Te} or/and R/L_{Ti}.

We can summarize the obtained trends within the description of the dependences of the density peaking on the heating systems, which has been already well investigated for positive R/L_n. In plasma scenarios with dominant ion heating which exhibit $R/L_{Ti} \geqslant R/L_{Te}$ [24, 25], we have ITG dominated regimes. For positive R/L_n, the particle flux is directed outward for a finite realistic collisionality. Such fluxes lead to a flattening of the density profile. In contrast, if starting from hollow profiles with $R/L_n < 0$, the particle flux is weak and becomes less inward as the collisionality increases, leading to slow evolution of the density profile. Increasing R/L_{Te} leads to a weaker outward flux for positive R/L_n and a stronger inward flux for $R/L_n < 0$. Therefore in case of dominant electron heating, the flattening of a peaked density profile is slowed down while the hollowness of a profile is expected to be reinforced as time passes by. Experimentally, in presence of dominant electron heating, as realized in Tore Supra and FTU experiments [26], more peaked density profiles at larger collisionality are reported.

Some general trends have been discussed here. It is shown that the particle flux can reverse sign and change its parametric trends depending on the initial conditions (low or high collisionality, dominant ion or electron heating, initially hollow or peaked density profiles, etc). These trends will be used as reference for the analysis of the particle flux of the self-consistent simulations with QuaLiKiz inside CRONOS presented in the next section. It can help in order to individuate the triggers of the density evolution and to highlight the behaviours governed by the theory, which can then be exploited for prediction of ITER.

4. Self-consistent time evolving simulations

The self-consistent simulation of the evolution of the electron density of the JET discharge 79676 just after the formation of the H-mode pedestal has been carried out using the quasi-linear gyrokinetic code QuaLiKiz [8] coupled to the transport code CRONOS [9].

At first, electron density and plasma current have been modelled self-consistently with the NBI deposition profiles, while keeping the temperatures and all the other quantities fixed to their experimental values. Then a simulation has been carried out including the heat transport evolution as well: current, density and temperatures have been simulated, together with the self-consistent calculation of the NBI deposition profiles.

The aim of the self-consistent simulations here presented is to model the transient evolution of the hollow density which characterizes the plasma core, through the core physics based transport model QuaLiKiz. For this reason appropriate boundary conditions have been chosen in order to obtain the sustainment of the density pedestal. Indeed, to carry out comprehensive physics based simulations of both the core and the edge region, all the relevant edge phenomena have to be included self-consistently. However, though several efforts have led to important progress in the field of the edge transport physics [27–29], nowadays there are no reliable transport models for the peripheral region of the plasma (i.e. the edge transport barrier region for H-mode plasmas).

The density pedestal has then been modelled taking ad hoc turbulent transport coefficients in the edge plasma region (between $\rho_{tn} = 0.93$ and $\rho_{tn} = 1$). Zero turbulent particle transport coefficients at the last closed flux surface (LCFS) and smooth continuity with the particle transport coefficients values calculated by QuaLiKiz at the normalized toroidal flux coordinate $\rho_{tn} = 0.93$ have been imposed. No edge recycling has been added, though the experimental discharge is characterized by a significant gas fuelling. Edge localized modes (ELMs) have been not included in the simulations.

Neoclassical transport has been included self-consistently in the simulation. The code NCLASS [30] has been used to calculate the neoclassical transport coefficients, which have been added to the turbulent transport coefficients on all the radial profile.

NBI deposition profiles have been calculated self-consistently in the simulation using the codes NEMO/SPOT [11].

Inside $\rho_{tn} = 0.25$, an ad hoc turbulent particle transport coefficient has been imposed in order to avoid numerical problems close to the centre of the plasma. Indeed, in the very core, the gradient lengths become lower than the critical thresholds and there is a systematic underestimation of the turbulence level by quasilinear codes such as QuaLiKiz [31]. From very recent studies [32], viable candidates for explaining at least part of such under-predictions are multi-scale turbulence mechanisms, which however are not included in the quasi-linear models.

To avoid the domains where the transport predictions might not be accurate enough due to the abovementioned turbulence underestimation at the very core and due to the influence of the cold neutral ionization source at the very edge which has not been considered in the simulations, the discussion hereafter is focused on the radial region $0.25 < \rho_{tn} < 0.93$.

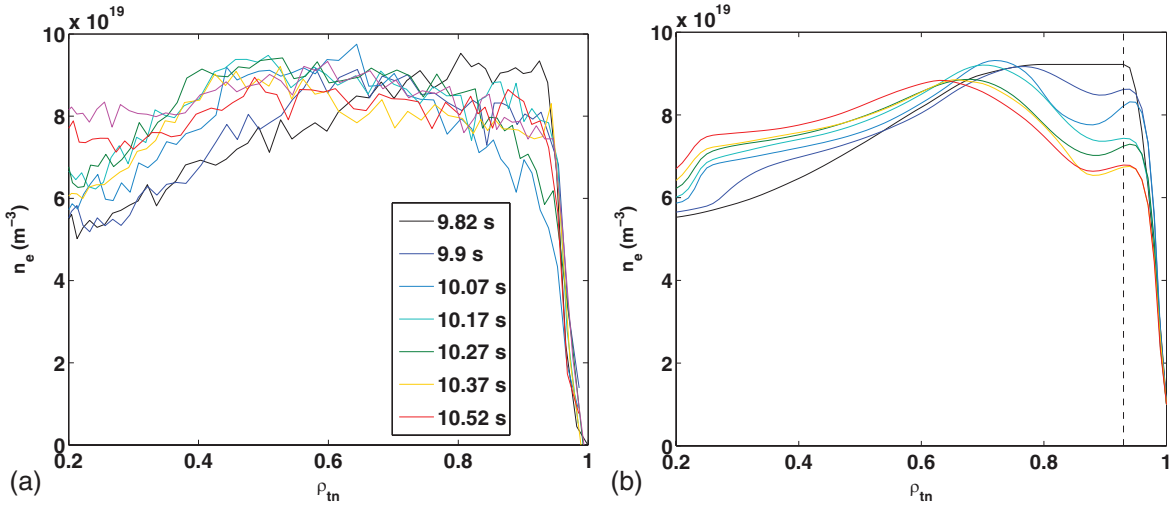

Figure 8. Evolution of the density profile in the experimental discharge (*a*) and as obtained by the simulation (*b*). Different colours correspond to the times of the legend of (*a*). The experimental density profile at 10.6 s, after the first sawtooth, is included in the graph (*a*) with the purple colour. The dashed line of (*b*) corresponds to the radial location of the imposed boundary conditions: $\rho_{tn} = 0.93$.

4.1. Self-consistent time evolving simulation: density and current

In figure 8, the results of the density-only simulation are shown together with the experimental density evolution. The experimental density pedestal is completely built within $1\tau_E$ after the L–H transition (not simulated), while the core density is characterized by a slower growth. This causes the formation of a hollow density profile, which tends to relax on slower timescale. This slow evolution is interrupted by a sawtooth event which takes place at $t = 10.6$ s. The experimental and simulated density profiles are shown from the time $t = 9.8$ s (just after the density pedestal formation) to the time just before the first sawtooth (10.55 s). The magenta line on the experimental density figure 8(*a*) is the density profile measured after the first sawtooth.

The boundary conditions imposed for the turbulent transport are enough to sustain the density pedestal and provide density values quite similar to the experimental ones at the top of the pedestal as illustrated by figure 8(*b*).

The dynamics of the maximum of the density profile is comparable in the simulation and in the experiment, showing an inward shift of this maximum on a similar time scale. In the simulation the maximum density ends up at the radial position $\rho_{tn} = 0.6$, the experimental density maximum is around $\rho_{tn} = 0.5$.

In the inner region, where the density profile remains hollow, the density increases significantly both in the experiment and in the simulation up to nearly $t = 10$ s. After that time, the simulation shows a much slower growth of the density, which seems to be due principally to the hollow NBI particle source and to the weak particle flux in the hollow part of the density profile.

The qualitative behaviour of the density peak and of the density profile in the negative R/L_n region has been checked to not depend on the imposed values and evolution of the density pedestal. In particular the density peak penetration position evolves as figure 8(*b*) shows, even with density pedestal values closer to the experimental ones. One possible reason of the differences between the predicted and the experimental density penetration depth could be the underestimation of the quasilinear particle flux shown in figure 4. However, additional studies are needed to address the origin of the quantitative discrepancies of the simulated results with respect to the experimental profiles.

In order to investigate the behaviour of the particle transport, first we have analysed the evolution of the terms of the continuity equation to evaluate which are the main contributors to the density evolution. Such equation can be written as:

$$\frac{R}{L_{ne}} = -\frac{RV_{TOT}}{D_{TOT}} + \frac{R}{V'|\nabla\rho|^2 D_{TOT} n_e}\int_0^{\rho}\left(SV' - \frac{\partial}{\partial t}(V' n_e)\right)\mathrm{d}\rho, \tag{2}$$

where V_{TOT} is the total convection, V' is the derivative of the plasma volume, S is the NBI particle deposition. All the terms are normalized to $R/n_e D_{TOT}$. V_{TOT} and D_{TOT} include the neoclassical contributions, which, however, are lower by 3–4 orders of magnitude than their turbulent counter-parts.

The evolution of the three terms on the right hand side of the continuity equation is represented in figure 9 at three different radial positions: $\rho_{tn} = 0.3$, $\rho_{tn} = 0.55$ and $\rho_{tn} = 0.8$.

In the inner part of the plasma ($\rho_{tn} = 0.3$, figure 9(*a*) and $\rho_{tn} = 0.55$, figure 9(*b*)), we see that, after $t = 10$ s, the particle source integral is nearly compensated by the density time derivative integral. It means that the particle input from sources directly translates into a local $\partial n_e/\partial t$ term with little transport. The total flux is indeed very small. At $\rho_{tn} = 0.3$, the convection is outward and lower with respect to the diffusion, the source and the n_e time derivative terms. This leads to a small and negative density peaking. At $\rho_{tn} = 0.55$, the density peaking is negative and larger, due to a larger outward convection term.

In the outer region of the plasma ($\rho_{tn} = 0.8$, figure 9(*c*)), the temporal variation of the density is alternatively negative and positive. A negative $\partial n_e/\partial t$ means that a strong outward

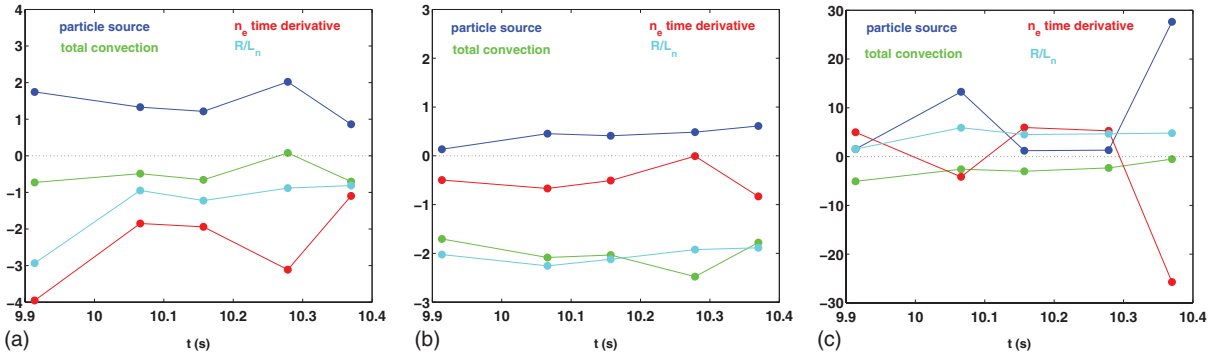

Figure 9. Time evolution of the R/L_{ne} (light blue points) and of the three terms on the right of the equation (2): the source term $\frac{R}{V'|\nabla\rho|^2 Dn_{\mathrm{e}}}\int_0^{\rho} SV'\mathrm{d}\rho$ (blue points), the density time derivative term $-\frac{R}{V'|\nabla\rho|^2 Dn_{\mathrm{e}}}\int_0^{\rho}\frac{\partial}{\partial t}(V'n_{\mathrm{e}})\mathrm{d}\rho$ (red points) and the total convection $-RV_{\mathrm{TOT}}/D_{\mathrm{TOT}}$ (green points). They refer to the discharge 79676 as obtained by the self-consistent simulation of the density-only at $\rho_{\mathrm{tn}} = 0.3$ (*a*), $\rho_{\mathrm{tn}} = 0.55$ (*b*) and $\rho_{\mathrm{tn}} = 0.8$ (*c*). The points are calculated at the times of figure 8, except the first and the last ones.

flux, made up of a diffusive and a convective part is contributing. Looking only at the times where $\partial n_{\mathrm{e}}/\partial t < 0$, we can see that the ratio between the total convection and the diffusion is reduced with time growing, leading to larger positive R/L_{ne}.

This analysis gives us the indication that, around $\rho_{\mathrm{tn}} = 0.3$, the density peaking time evolution is mainly determined by the source and the n_{e} derivative terms, which are dominant with respect to the turbulent transport coefficients. On the contrary, the region close to $\rho_{\mathrm{tn}} = 0.55$ is dominated by turbulent transport. At $\rho_{\mathrm{tn}} = 0.8$, for negative $\partial n_{\mathrm{e}}/\partial t$ all the terms are equally important, for positive $\partial n_{\mathrm{e}}/\partial t$ the turbulent coefficients are nearly negligible, due to the prediction of a very low instability.

Except for the inner part of the plasma, the turbulent transport plays a relevant role both in the negative and in the positive R/L_n regions. The computed turbulent particle fluxes and their components have been investigated: diffusion and convection (including compressibility and thermodiffusion) are directly provided by QuaLiKiz by integrating separately the various quasilinear gyrokinetic flux contributions. In figure 10, the modelled total particle fluxes, the convective contributions and the diffusive parts are shown for the times of figure 8.

Looking at the time evolution of the modelled density profiles (figure 8(*b*)) and of the various parts of the particle fluxes (figure 10), we can distinguish three radial regions to deepen the analysis: the edge region ($0.85 < \rho_{\mathrm{tn}} < 0.95$), the region where the density slowly peaks ($0.6 < \rho_{\mathrm{tn}} < 0.85$) and the $R/L_n < 0$ region ($0.3 < \rho_{\mathrm{tn}} < 0.6$).

In the edge region, we have an outward particle flux at all times. In this region, large R/L_{T} and R/L_n, due to the pedestal, are driving large outward diffusions and convections. That is visible in figure 11, where the R/L_{T} and R/L_n profiles, together with the coefficients of the particle transport are shown for the first time step $t = 9.82$ s (Here, and for all the following plots, the major radius R is taken constant, $R = 3$ m) At $\rho_{\mathrm{tn}} = 0.85$–$0.93$, the density is flattened and R/L_n is close to zero. At this location, we are in an ITG dominated regime, where the compressibility dominates over the thermodiffusion and is directed outward as illustrated by figure 11. It is due to the high collisionality in this region ($\nu^* > 0.2$), hence, in spite of the high R/L_{Te}, the trapped particles do not contribute much, leading to a weak curvature and ∇B inward convection (see figure A1 and table A1 in the appendix). For $0.93 < \rho_{\mathrm{tn}} < 0.95$, R/L_n has high positive values. In this case, the dominant instabilities are TEM, and the thermodiffusion coefficient dominates over the inward compressibility, giving an outward flux, as expected by the theory (see figure A2). However, in the self-consistent simulation, for $\rho_{\mathrm{tn}} > 0.93$ $\rho_{\mathrm{tn}} > 0.93$, the imposed boundary conditions dominate the particle transport.

In the region $0.6 < \rho_{\mathrm{tn}} < 0.85$, we find particle fluxes alternatively equal to zero or positive as illustrated on figure 10. That happens for both the convective and the diffusive parts. We consider the time $t = 10.17$ s, for which we find a finite particle flux due to dominant ITG instabilities. At that time, we look at the diffusion and convection contributions shown in figure 12 with their corresponding R/L_n, $R/L_{\mathrm{Ti,e}}$ profiles. The compressibility is always positive and dominates. The thermodiffusion changes sign from negative to positive in a zone in which R/L_n varies significantly as it is shown in figure 12(*a*). Even the collisionality is increasing, from $\nu^* = 0.046$ in $\rho_{\mathrm{tn}} = 0.7$ to $\nu^* = 0.082$ in $\rho_{\mathrm{tn}} = 0.8$. The behaviour of the particle transport coefficients around $\rho_{\mathrm{tn}} = 0.7$ falls within the cases theoretically foreseen for negative and low positive R/L_n at intermediate collisionality (see figures A1–A3). The positive thermodiffusion is typical of a high positive R/L_n, as expected for high collisional ITG regimes (see figures A1–A3). The time oscillation from zero to positive fluxes in this radial region is a sign for the high sensitivity of the particle flux to the R/L_n and R/L_{T} profiles as well as a sign of the vicinity to the stability limit. However, on average, the flux is outward, and the particles are flowing out of this region.

In the inner half of the plasma ($0.3 < \rho_{\mathrm{tn}} < 0.6$), the hollow density is slowly evolving, because of very low particle flux and source. As figure 10 shows, the particle flux remains low due to the compensation between the convective and the diffusive parts. The particle flux starts being slightly inward in the first time steps, and becomes slightly outward at later times.

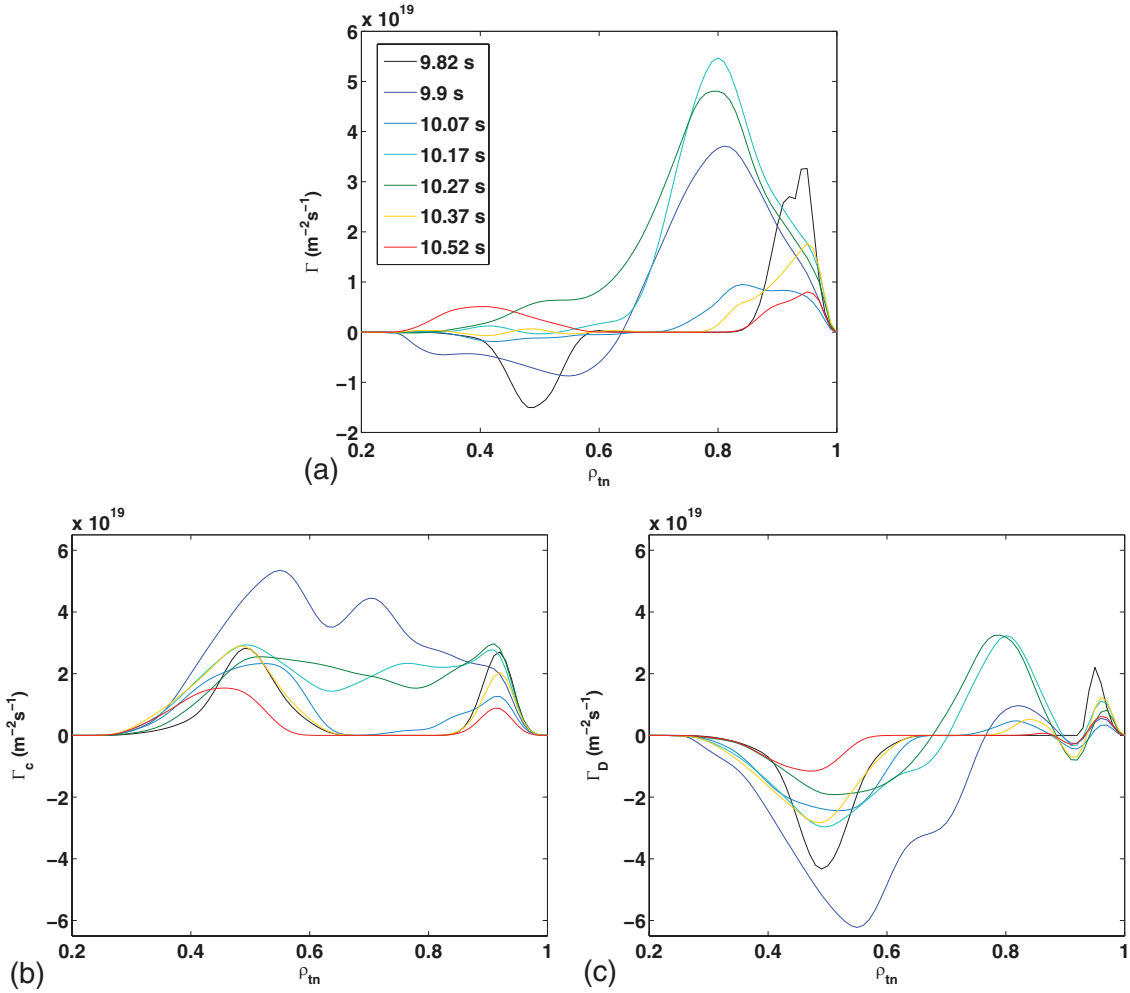

Figure 10. Evolution of the particle fluxes relative to the density profiles of figure 8. The total particle flux (*a*), the convection (*b*) and the diffusion (*c*) contributions as calculated by QuaLiKiz used self-consistently with CRONOS.

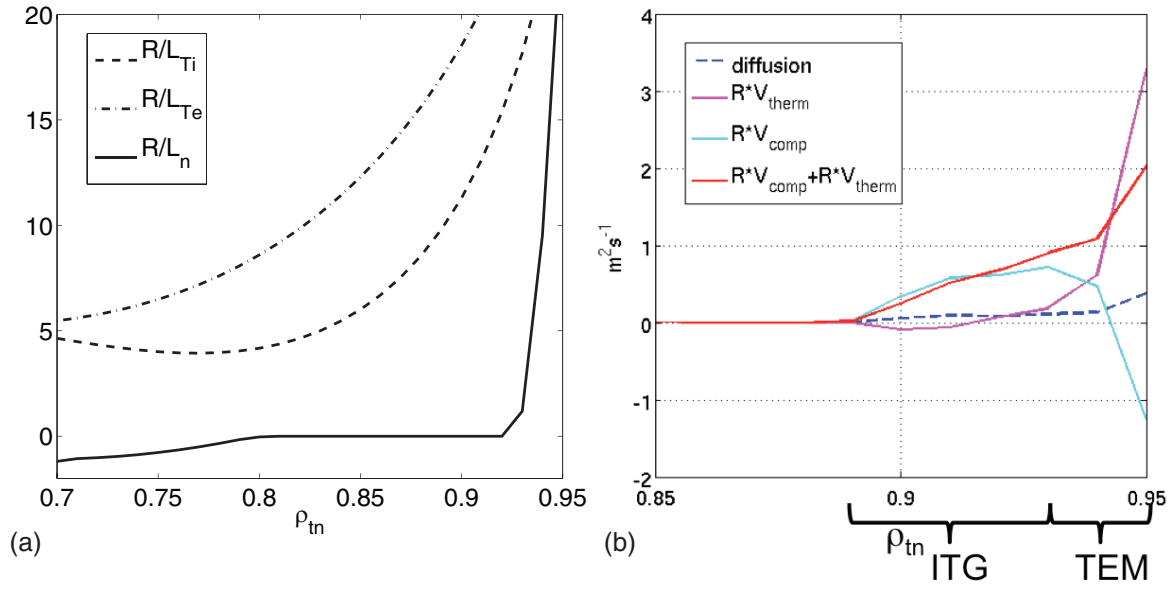

Figure 11. (*a*) R/L_n, R/L_{Ti} and R/L_{Te} profiles in the outer region of the discharge 79676 at 9.8 s. (*b*) Particle transport coefficients for the same outer region.

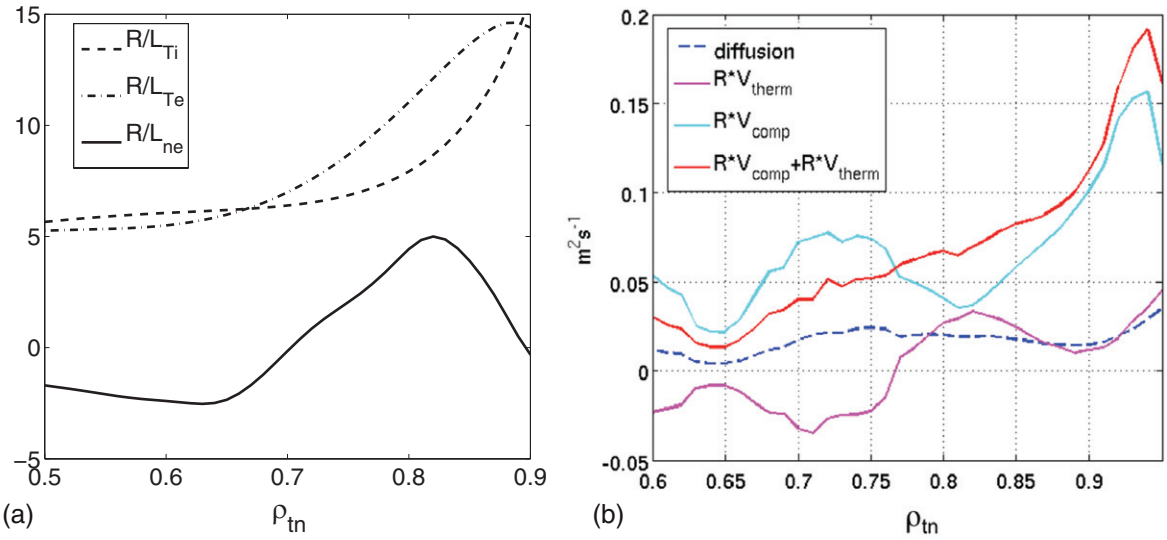

Figure 12. (*a*) R/L_{ne}, R/L_{Ti} and R/L_{Te} profiles in the density peak region of the discharge 79676 at the time 10.17 s. (*b*) Particle flux coefficients profiles in the density peak region of the discharge 79676 at the time 10.17 s.

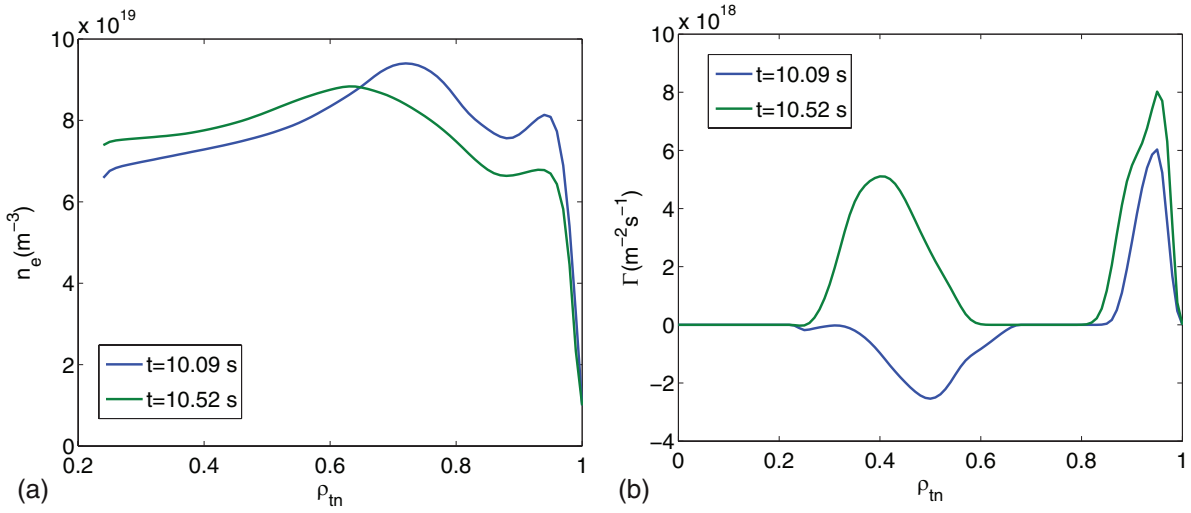

Figure 13. (*a*) Density and (*b*) relative particle fluxes profiles for the discharge 79676 at the times 10.09 s and 10.52 s.

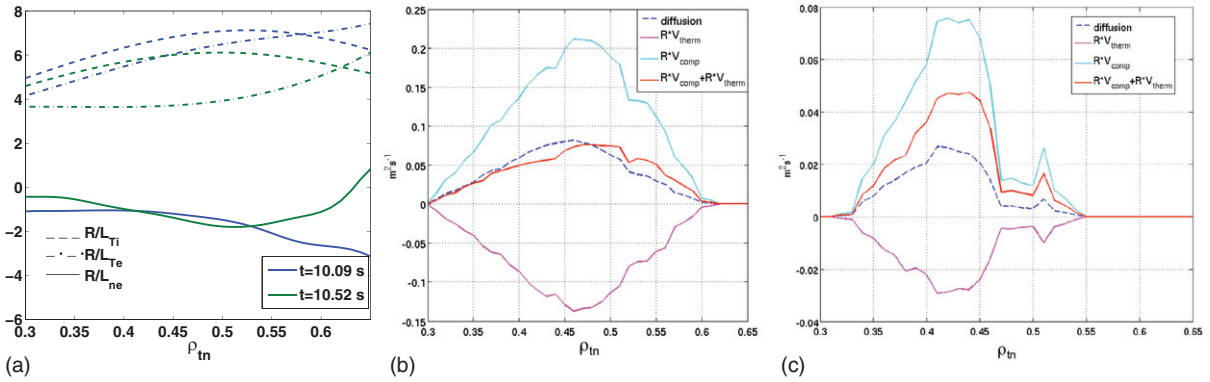

Figure 14. (*a*) R/L_{Ti}, R/L_{Te} and R/L_n profiles in the negative R/L_n region of the discharge 79676 at the times 10.09 s (blue) and 10.52 s (green). Particle flux coefficients profiles in the negative R/L_n region of the JET discharge 79676 at the times 10.09 s (*b*) and 10.52 s (c).

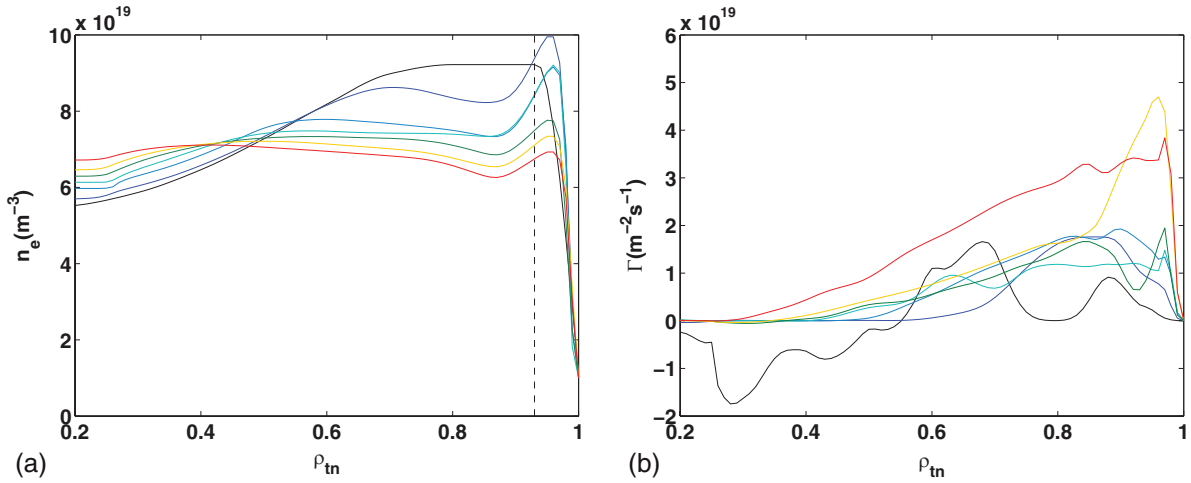

Figure 15. Evolution of the density profile (*a*) and of the relative particle fluxes (*b*) of the JET discharge 79676, as obtained by modelling self-consistently density, temperatures and current. The dashed line of (*a*) corresponds to the radial location of the imposed boundary conditions: $\rho_{tn} = 0.93$.

In figure 13, we consider two density profiles at two different times, where the particle fluxes have opposite direction in the region between $\rho_{tn} = 0.35$ and $\rho_{tn} = 0.6$. The relative $R/L_{Ti,e}$ and R/L_n profiles are reported in figure 14(*a*). R/L_n is similar for the two cases, while R/L_{Te} is higher at the 10.09 s than at 10.52 s. The values of ν^* are similarly low for the two times ($\nu^* \sim 0.015$). While the compressibility and the diffusivity do not depend on the R/L_{Te} values for negative R/L_n, the thermodiffusivity is reduced for smaller R/L_{Te}, leading then to a weaker flux, which can also be outward for low finite ν^* (see figure A5).

Looking at figures 14(*b*) and (*c*), where the particle transport coefficients are shown for both times, we see that at the earlier time, when R/L_{Te} is higher, the diffusion and the total convection compensate each other, leading to a negative flux because of a negative density gradient, $R/L_{ne} < -1$. At the later time, the thermodiffusion is less influent and the outward compressibility dominates, giving a total convection higher than the diffusion, hence an overall outward total flux.

The low level of particle flux (even outward after $t = 10.2$ s) in the $R/L_n < 0$ region, in conjunction with the low particle source from NBI, explains the quasi-frozen dynamics of the density profile which stays hollow in the inner half over the whole simulation. This feature seems to be supported by the experiment, in which the hollowness of the density profile stays until it is affected by a sawtooth event. That means that the sawtooth event plays a decisive role in the sudden flattening of the density profile in the experiment at $t = 10.6$ s, which would have taken much longer time with turbulent transport only. This suggests that, in ITER, where both the turbulent transport time scales and the sawtooth period will be longer than in JET, the density profile could remain hollow over a long time if the q-profile is shaped to avoid core MHD activity once the L–H transition is triggered. However, because of the uncertainty about the appearance and the maintenance of transient hollow density profiles after the L–H transition in ITER, dedicated transport modelling studies on the assessment of this possible configuration and on the dependences on fuelling conditions are required.

4.2. Self-consistent time evolving simulation: density, temperatures and current

We now turn to the self-consistent simulation of electron density, current density and ion and electron temperatures. The temperature pedestal has been modelled using the model KIAUTO [33], which calculates the pedestal height using the critical pressure gradient. Figure 15 shows the calculated density profiles and the corresponding particle fluxes. The flux is always outward in the region of the density peaking ($\rho_{tn} = 0.6 - 0.8$). This region is shifted more inside the plasma, in a way closer to the experiment. However, in these simulations, we see the density peaking decreasing while shifted. In the negative R/L_n more central region, the flux, which is extremely low, changes from inward to outward, similarly to the simulation described above. As a consequence, the hollow profile is filled faster than in the experiment.

In figures 16 and 17, the simulated ion and electron temperature profiles are compared to the experimental data for the times corresponding to the density evolution of figure 15. For times up to 10 s, a good agreement between experimental and simulated temperatures is obtained. After 10 s, simulated ion and electron temperature profiles start to overestimate the experimental ones. Larger R/L_T values are obtained by the simulation. They are further above the stability threshold than the experimental ones. The simulated larger R/L_T values then cause an outward particle flux which is responsible of the decrease of the n_e peak. After 10.1 s, the temperatures increase is very slow, similarly to the experimental evolution. The temperature overestimation by the model could be due to (1) uncertainties in the NBI deposition power calculation, (2) underestimated quasilinear heat flux when compared to their nonlinear counterparts (see section 2.1), (3) underestimated turbulent heat transport in the edge region.

5. Summary and conclusions

In this paper, the slow flattening of the hollow density during the transient phase after the L–H transition of the high current

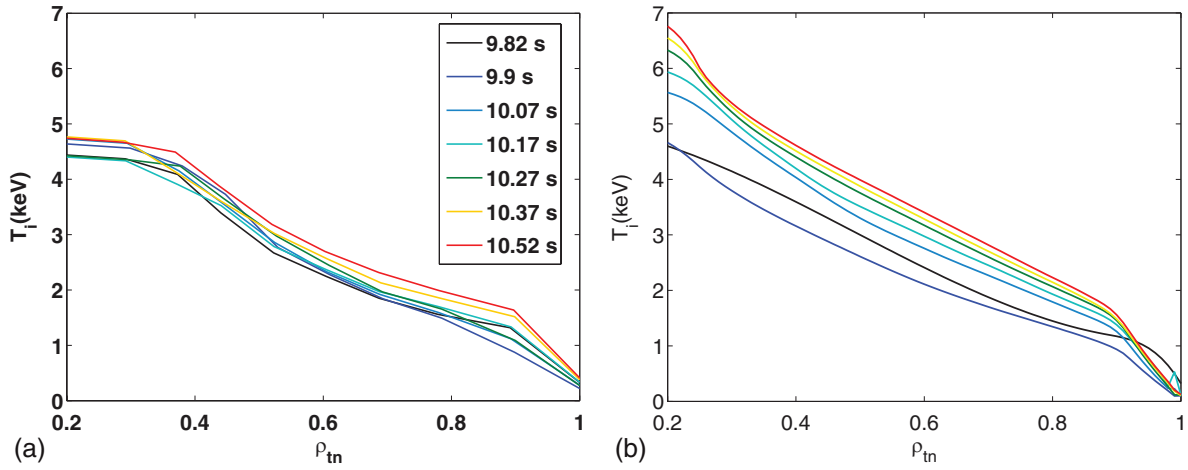

Figure 16. Experimental (*a*) and simulated (*b*) ion temperature profiles of the JET discharge 79676. Different colours correspond to the times of the legend of figure (*a*).

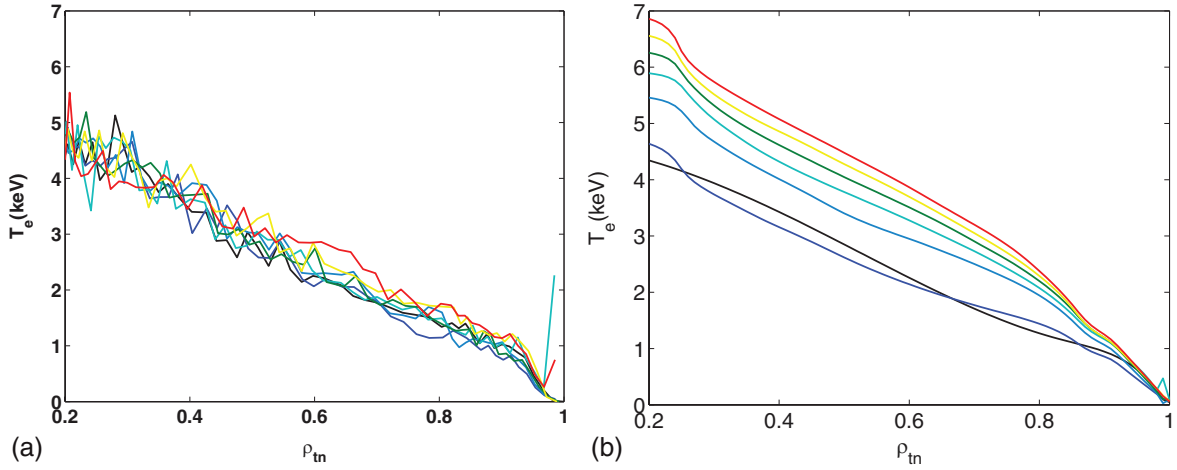

Figure 17. Experimental (*a*) and simulated (*b*) electron temperature profiles of the JET discharge 79676. Different colours correspond to the times of the legend of (*a*).

JET carbon discharge 79676 has been investigated. This study is motivated by the ITER relevance of this discharge, and by the particular density evolution, which has been found to be beneficial in the view to the H-mode access in ITER [4].

The quasilinear gyrokinetic code QuaLiKiz [8] has been used both in its stand-alone version and self-consistently with the transport code CRONOS [9].

A benchmark between QuaLiKiz and the more comprehensive gyrokinetic code GKW has been carried out including hollow density profile cases where $R/L_n < 0$. QuaLiKiz particle fluxes agree with the quasi-linear GKW results, while a discrepancy between quasi linear and nonlinear GKW results has been found. It is due to a difference in the calculation of the ion heat flux, used for the normalization of the saturation amplitude in the quasilinear model. Future investigations are planned at a later stage.

QuaLiKiz has then been used to deepen the stand-alone analysis. The dependences of the particle flux contributions (diffusion, thermodiffusion, compressibility) have been studied for positive and negative R/L_n. As expected by theory, and in agreement with [14], TEM are fully stable at $R/L_n < 0$. The particle flux amplitude and direction are shown to be highly sensitive to the density gradient sign, to the collisionality, to the temperature gradient length as well as to the ratio of ion to electron heating. As a result, in view to extrapolate towards ITER particle transport, it is fundamental to account self-consistently for collisionality, ratio of R/L_{Te} to R/L_{Ti}, values and sign of R/L_n, which all together concur to the particle flux.

QuaLiKiz has then been used coupled to the transport code CRONOS to self-consistently model the JET discharge 79676. Letting evolve the density and the current, we have found that, inside $\rho_{\mathrm{tn}} = 0.55$, where the density evolves slowly and remains hollow, the simulation well reproduces the reported density behaviour. In conjunction with the low NBI particle source, the resulting density evolution is quite slow and the hollowness of the density profile stays over the whole duration of the simulation. This is consistent with the experiment where the density profile is flattened by a sawtooth event shortcutting the slow turbulent transport processes. In the outer region ($\rho_{\mathrm{tn}} > 0.55$), the modelling reproduces a density peak shifting towards the inner part of the plasma, as observed in the experiment.

Table A1. Direction of the electron convection terms in the curvature and slab quasi-linear limits (table taken from [8]).

	Electrons			
	Compressibility		Thermodiffusion	
	Electron turbulence (TEM)	Ion turbulence (ITG)	Electron turbulence (TEM)	Ion turbulence (ITG)
Curvature only	Inward *Outward if* $s << 0$ *or* $\alpha >> 1$		Outward *Inward if* $s << 0$ *or* $\alpha >> 1$	Inward *Outward if* $s << 0$ *or* $\alpha >> 1$
Slab limit	Inward	Outward	Inward	

The simulation evolving the ion and electron temperatures as well as the density and the current has given a similar, though stronger, trend. The particle flux is outward at all times outside $\rho_{tn} = 0.5$. The density peaking is shifted towards more inner locations. However the modelled density peaking is weaker than the experimental case. The temperatures, initially well reproduced, are overestimated during the simulation.

The obtained results are highly sensitive to the values of R/L_T, R/L_n and to the collisionality. In particular, the excited modes, and then the resulting fluxes, strongly depend on parameters like the normalized temperature gradients, which in self-consistent simulations can differ significantly from the experimental ones, although the resulting temperatures are not so far from the experimental values. Furthermore, these simulations try to reproduce a transient phase where particle sources and fluxes in the inner half of the plasma are small and the turbulence close to marginal stability. Finally, important physical phenomena as the ELMs have not been included in the simulation. By expelling particles from the edge, they can influence in a non-negligible way the simulated quantities. For example, the first part of the evolution of the density peak, which is close to the edge in the investigated JET discharge, could be affected by such events.

Although the complex mechanism of the density evolution in the transient phase of the JET discharge 79676 is not reproduced in a comprehensive way, the self-consistent density simulations presented here reproduce the slow evolution of the hollow density in the core of the plasma. This good description of the core evolution is due to a prediction of the behaviour of the turbulent particle transport coefficients, which, in the case of $R/L_n < 0$, differs from the better known and investigated behaviour at $R/L_n > 0$. In particular the particle flux amplitude is reduced for negative R/L_n. The reproduced slow evolution seems to have a quite general physics basis as it follows from the theory-based simulations and the stand alone analysis presented here. In the experiment, the sawtooth event is found to play a decisive role in the sudden flattening of the density profile at $t = 10.6$ s, which would have taken longer with turbulent transport only. This suggests that, in ITER, where the turbulent transport time scales will be longer than in JET, the density profile may stay hollow over a long time if the q-profile is shaped to avoid core MHD activity once the L–H transition is triggered.

This work opens new perspectives for self-consistent simulations of the transient density build-up in ITER scenarios using first-principles transport models, with boundary conditions at the LCFS. It remains important to continue the effort on understanding the comprehensive mechanism of the evolution of the density in this transient phase in existing machines. To move forward towards more quantitative predictions, it is essential to include edge particle source models in addition to the NBI deposition particles source.

Acknowledgments

The authors thank G. Staebler and Y. Camenen for stimulating discussions. This work has been carried out within the framework of the EUROfusion Consortium and has received funding from the European Union's Horizon 2020 research and innovation programme under grant agreement number 633053. The views and opinions expressed herein do not necessarily reflect those of the European Commission or those of the ITER Organization.

Appendix

The two convection mechanisms, compressibility and thermodiffusion, have been widely investigated through theoretical analyses and experimental studies. As it is summarized in table A1, the compressibility convection is made of two terms: the parallel compressibility [8, 34] and the curvature and ∇B drifts (also known as TEP, see [35, 36]). The curvature and ∇B drift is always directed inward. Experiments where the density peaking was reported to scale strongly with $\nabla q/q$ [24] or with the internal inductance in H and L modes [37], are consistent with dominant curvature and ∇B drift. In such cases, reduced trapped particles contribution due to larger collisionality is expected to lead to weaker inward convection, hence flatter density profiles. Such collisionality dependences are reported in [24, 37–39]. Nonetheless this trend is not universal, indeed for example in the large collisionality FTU pulses [26], the convection velocity seemed to be dominated by the thermodiffusion. In such cases, the collisionality increase leads to less TEM and more ITG, leading to a larger inward thermodiffusion, the density peaking is indeed reported to increase for larger collisionalities.

The strength and the direction of the convection is then known to be affected by several physics parameters. In the following we use QuaLiKiz in order to investigate the parametric dependences of the convective coefficients and of the total particle flux on the collisionality, R/L_T and R/L_{Ti} versus R/L_{Te}, quantities which are known to influence the particle flux. The impact of these parameters is investigated for negative R/L_n, and compared with the already well investigated results obtained with positive R/L_n [3, 13]. Their influence on the convection, on the diffusivity part and on the total particle

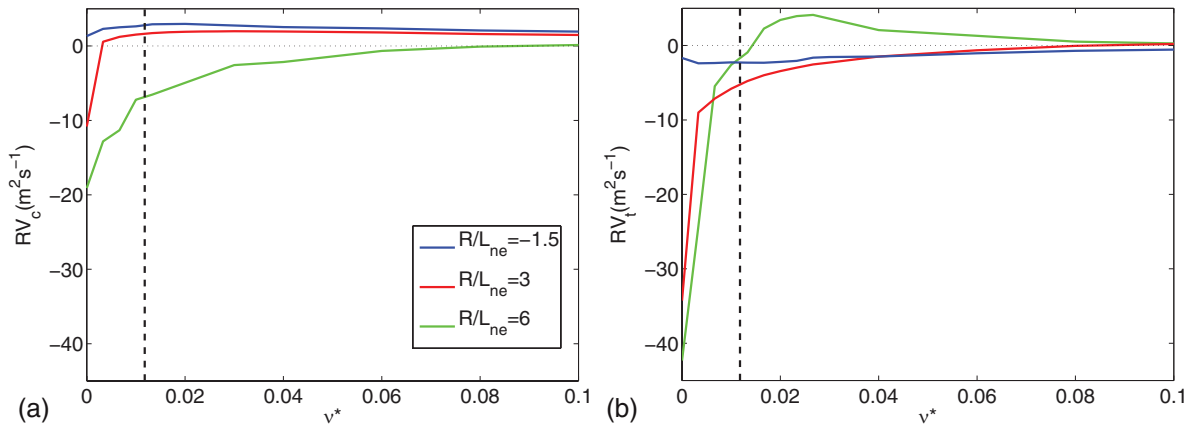

Figure A1. (*a*) Compressibility and (*b*) thermodiffusion plotted as a function of ν^* for R/L_n =6 (green line), R/L_n =3 (red line) and $R/L_n = -1.5$ (blue line). The dashed line represents the collisionality $\nu^* = 0.0118$, calculated using the set of parameters of table 1.

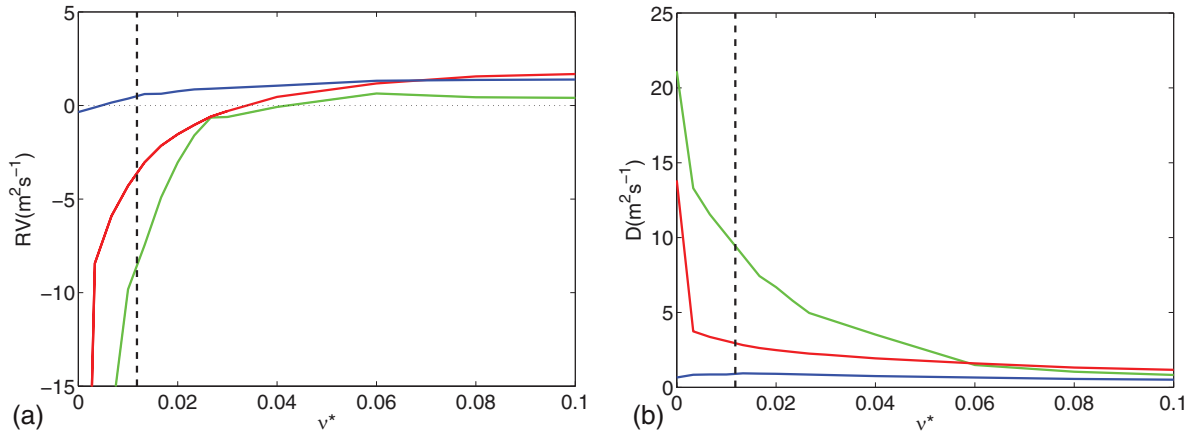

Figure A2. (*a*) Total convection and (*b*) diffusion as functions of ν^* for $R/L_n = 6$ (green line), for R/L_n =3 (red line) and $R/L_n = -1.5$ (blue line). The dashed line represents the collisionality $\nu^* = 0.0118$, calculated using the set of parameters of table 1.

flux is here shown and explained while referring to the dominant instabilities. The parameters reported in table 1 are used as a basis for the parametric scans. First we present a scan of the collisionality for different R/L_n (-1.5, 3 and 6), taking $R/L_{\rm Ti} = R/L_{\rm Te} = 6$, values expected for the ITER baseline scenario, as reported in section 2.

In figure A1(*a*) the compressibility is shown as a function of the collisionality for the three investigated values of R/L_n. In the case of $R/L_n = -1.5$, we find a compressibility always outward for the whole investigated interval of $\nu*$ values. At $\nu^* \sim 0$, ITG modes dominate, as illustrated in figure 7, hence the compressibility is outward because of the prevalence of the parallel compressibility (table A1). For positive R/L_n, we recover the behaviour described in [3, 23]: the compressibility changes sign (from negative to positive) at values of $\nu*$ which grow with increasing R/L_n. At $\nu^* \sim 0$, the effect of the trapped electrons is dominant, leading to an inward compressibility (see table A1). For $\nu^* > 0$, the contribution of trapped electrons becomes weaker, and, for both negative and positive R/L_n, we have an outward compressibility, due to the parallel compressibility carried by dominant ITG.

The respective thermodiffusion terms are shown in figure A1(*b*). For low values of ν^* the thermodiffusion is negative for all the investigated R/L_n. It tends to become more

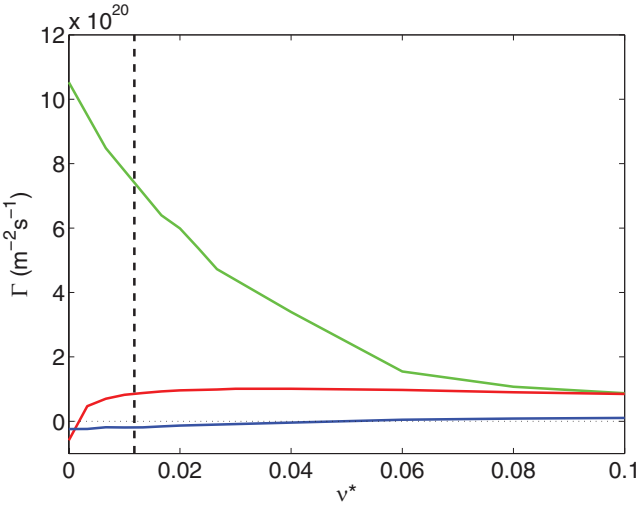

Figure A3. Total particle flux as a function of $\nu*$ for $R/L_n = 6$ (green line), $R/L_n = 3$ (red line) and $R/L_n = -1.5$ (blue line). The dashed line represents the collisionality $\nu^* = 0.0118$, calculated using the set of parameters of table 1.

easily outward as R/L_n is increased. This is due to a larger TEM contribution at higher R/L_n, leading to an outward thermodiffusion (see table A1). For high $\nu*$, ion turbulence

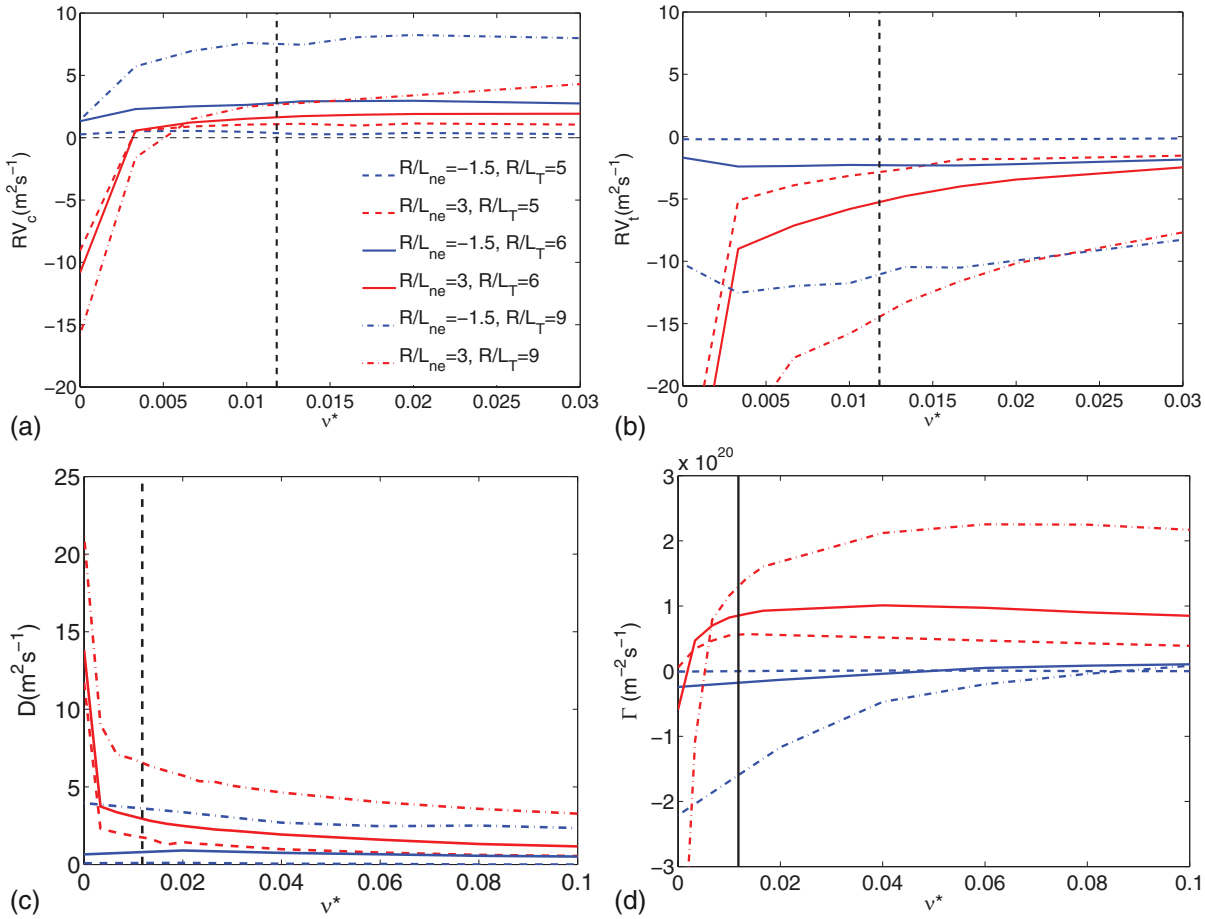

Figure A4. (*a*) Compressibility, (*b*) thermodiffusion, (*c*) diffusivity and (*d*) total particle flux as functions of $\nu*$ for $R/L_n = 3$ (red lines) and $R/L_n = -1.5$ (blue lines) for different R/L_T values. The black dashed line represents the collisionality $\nu* = 0.0118$, calculated using the set of parameters of table 1.

is dominant for all the investigated R/L_n, and the thermodiffusion, if inward, tends to decrease in strength with the collisionality, in agreement with the gyrokinetic calculations reported in [13, 40]. However, as [41] has obtained, in a high collisionality ITG regime an outward thermodiffusion can be found in presence of a high enough R/L_n with respect to R/L_{Te}. Parameter relations, as the ratio $(R/L_n)/(R/L_{Te})$, influence the mode dominance, as well as the strength and the direction of the thermodiffusion: it indeed can decreases with $\nu*$, as for the cases shown in figure A1(*b*), or can increases with $\nu*$, as for the FTU experimental case above mentioned.

As shown in figure A2(*a*), for negative R/L_n, the total convection is outward and low, while for positive R/L_n it is inward at low collisionality, with a higher absolute value with increasing R/L_n. As the collisionality increases, it becomes outward and remains low for all R/L_n values. The diffusivity coefficient illustrated by figure A2(*b*) decreases with increasing collisionality. The trend is more pronounced for higher positive R/L_n, less so for negative R/L_n. Indeed, the stabilizing impact of $\nu*$ is indeed smaller for cases having weaker TEM contribution, i.e. $R/L_n < 0$.

On figure A3 the total particle flux is illustrated. For $R/L_n = -1.5$ it is low and inward for small collisionalities, decreasing in absolute value as $\nu*$ increases until becoming directed outward. For $R/L_n = 3$, we find the behaviour reported in [3], characterized, in absence of collisionality, by a negative flux, which inverts its sign, becoming outward, for very low values of $\nu*$. The flux of the $R/L_n = 6$ case is high and positive for $\nu* = 0$, and decreases with increasing collisionality because of the dominance of the diffusion part.

Therefore, the collisionality influences differently the particle flux for different R/L_n. In particular, for negative R/L_n the flux remains low and inward for values of collisionality typical of real experiments, while it does not happen for $R/L_n > 0$, where an outward flux characterizes finite collisionality cases.

Now we will study the impact of R/L_{Te} versus R/L_{Ti} on the particle flux behaviour. Indeed, changing the values and the ratio between R/L_{Ti} and R/L_{Te} can lead to important changes to the nature of dominant modes and to hence to the particle flux [3, 13, 23].

At first, we keep fixed the ratio $R/L_{Te}/R/L_{Ti} = 1$ and change the values of the normalized temperature gradient length from 4 to 9. In figure A4, the compressibility, the thermodiffusion, the diffusivity and the total particle flux are shown as functions of collisionality for different values of R/L_T and for two values of R/L_n: 3 and -1.5. The absolute value of the compressibility increases with increasing R/L_T, (see figure A4(*a*)) due to the reinforcement of the dominant instabilities (i.e. ITG for negative R/L_n and for positive R/L_n at high collisionality,

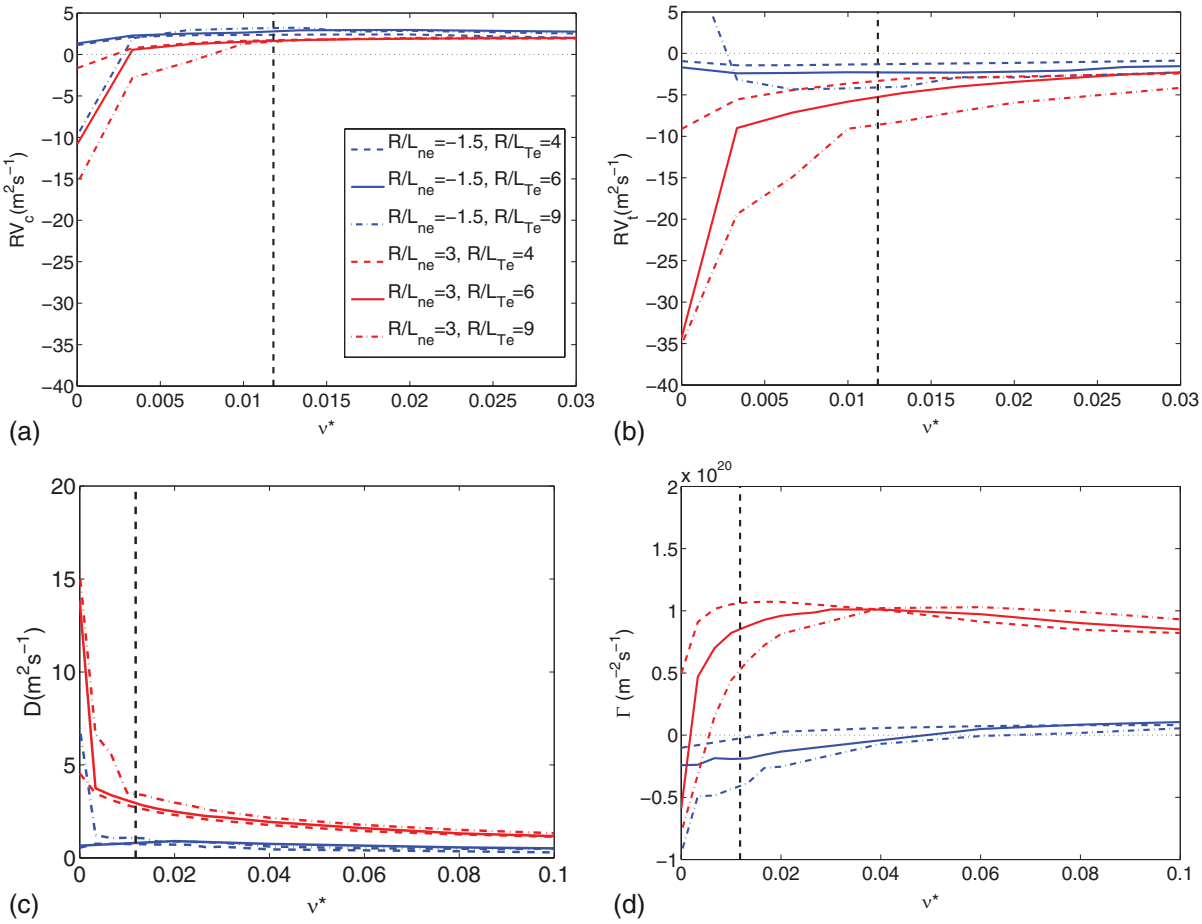

Figure A5. (*a*) Compressibility, (*b*) thermodiffusion, (*c*) diffusivity and (*d*) total particle flux as functions of $\nu*$ for $R/L_n = 3$ (red lines) and $R/L_n = -1.5$ (blue lines) for different R/L_{Te} values. The dashed line represents the collisionality $\nu^* = 0.0118$, calculated using the set of parameters of table 1.

TEM for positive R/L_n at low collisionality). The thermodiffusion (see figure A4(*b*)) is negative for all the values of R/L_n and R/L_{T} and is reduced with increasing R/L_{T}, because of stronger instabilities and since it scales with R/L_{Te} (see equation (1)). Then for negative R/L_n the total convection becomes larger and negative with increasing R/L_{T}.

Figure A4(*c*) shows the diffusivity which is affected by different R/L_{T} values, becoming higher with increased R/L_{T}.

In figure A4(*d*) we can see that the flux is stronger for larger R/L_{T}. While for positive R/L_n the sign inversion takes place for very low values of collisionality, for negative R/L_n the flux keeps to be inward over a large collisionality interval. With increasing R/L_{T} the interval becomes even larger, up to $\nu^* = 0.1$, including then a wide range of experimental cases. This behaviour is essentially due to the reinforcement of the already dominant ITG instabilities.

Now, if we fix R/L_{Te} and scan only R/L_{Ti}, we obtain a very similar trend with respect to the one described above. The particle transport is characterized by a stronger flux with increased R/L_{Ti} for both negative and positive R/L_n. However in this case the thermodiffusivity is less reinforced since R/L_{Te} stays constant. For $R/L_n < 0$, the major compensation between compressibility and thermodiffusion leads to a weaker total convection with respect to the case of $R/L_{\mathrm{Ti}} = R/L_{\mathrm{Te}} = 9$, and a weaker flux.

If we fix the value of $R/L_{\mathrm{Ti}} = 6$ and vary R/L_{Te} from 4 to 9 we obtain the compressibility, thermodiffusion, diffusivity and total particle flux shown in figure A5. In the case of negative R/L_n, for finite $\nu*$, the compressibility does not depend on R/L_{Te}. For positive R/L_n, the inward compressibility is reinforced by larger R/L_{Te} due to strengthened TEM. For high collisionalities, where the TEM effect is weaker, the differences in the compressibility for different R/L_{Te} become nearly negligible. By looking at the thermodiffusion shown in figure A5(*b*), we can see a shift towards more inward convection with increased R/L_{Te} with respect to R/L_{Ti}, for both positive and negative R/L_n: such difference remains relevant even for high collisionalities, like in the R/L_{T} scan. The total convection obtained by increasing R/L_{Te} has then a more inward trend with respect to the case of $R/L_{\mathrm{Te}} = R/L_{\mathrm{Ti}} = 6$, leading a stronger inward flux for $R/L_n < 0$.

In the case of negative R/L_n, the diffusivity does not depend on R/L_{Te}. For positive R/L_n, it grows with increasing R/L_{Te} in the range of very low $\nu*$.

The total particle fluxes are shown in figure A5(*d*). They change sign at larger values of ν^* for larger R/L_{Te}. In the case of positive R/L_n, it occurs at very low collisionalities, and, for collisionalities up to $\nu^* = 0.04$, the outward flux becomes lower with increasing R/L_{Te}. For negative R/L_n, the sign inversion takes place for different values of ν^* varying

R/L_{Te}. While at $R/L_{\mathrm{Te}} < R/L_{\mathrm{Ti}}$, the flux is low and outward on almost the whole investigated ν^* interval, with increasing R/L_{Te} a stronger inward flux is found for a larger interval of ν^*. This means that the collisionality impact on the particle flux depends on both the R/L_n sign and R/L_{Te} and R/L_{Ti} ratio. Such dependences have to be included when extrapolating towards ITER.

Here, we have shown that the convection changes sign depending on various parameters. In particular, the inward curvature and ∇B drift is easily dominated by the parallel compressibility which changes sign depending on the nature of the dominant unstable mode. The thermodiffusion term can also dominate over the total compressibility term and also changes sign. Therefore the overall particle flux can be inward or outward and responds differently to R/L_n, collisionality, $RL_{\mathrm{Ti,e}}$ values and ratio, meaning that extrapolations towards ITER have to include finite collisionality impact as well as to account for dependences on R/L_{Te} versus R/L_{Ti} and R/L_n. Hence the resulting density profiles can indeed be transiently hollow [4].

References

[1] Snipes J.A. *et al* 1996 *Nucl. Fusion* **36** 1217
[2] Garbet X. *et al* 2004 *Plasma Phys. Control. Fusion* **46** B557–74
[3] Angioni C. *et al* 2009 *Plasma Phys. Control. Fusion* **51** 124017
[4] Loarte A. *et al* 2013 *Nucl. Fusion* **53** 083031
[5] Nunes I. *et al* 2013 *Nucl. Fusion* **53** 073020
[6] Erba M. *et al* 1997 *Plasma Phys. Control. Fusion* **39** 261
[7] Garzotti L. *et al* 2003 *Nucl. Fusion* **43** 1829
[8] Bourdelle C. *et al* 2007 *Phys. Plasmas* **14** 112501
[9] Artaud J.F. *et al* 2010 *Nucl. Fusion* **50** 043001
[10] Peeters A.G. *et al* 2009 *Comput. Phys. Commun.* **180** 2650
[11] Schneider M. *et al* 2005 *Plasma Phys. Control. Fusion* **47** 2087
[12] Angioni C. *et al* 2011 *Nucl. Fusion* **51** 023006
[13] Fable E. *et al* 2010 *Plasma Phys. Control. Fusion* **52** 015007
[14] Garzotti L. *et al* 2014 *Plasma Phys. Control. Fusion* **56** 035004
[15] Casati A. *et al* 2009 *Nucl. Fusion* **49** 085012
[16] Casati A. 2009 A quasi-linear gyrokinetic transport model for tokamark plasmas *PhD Dissertation* Université de Provence
[17] Waltz R.E. *et al* 2009 *Phys. Plasmas* **16** 072303
[18] Gorler T. *et al* 2008 *Phys. Rev. Lett.* **100** 185002
[19] Dannert T. *et al* 2005 *Phys. Plasmas* **12** 072309
[20] Bourdelle C. *et al* 2002 *Nucl. Fusion* **42** 892
[21] Angioni C. *et al* 2012 *Nucl. Fusion* **52** 114003
[22] Angioni C. *et al* 2009 *Phys. Plasmas* **16** 060702
[23] Angioni C. *et al* 2005 *Phys. Plasmas* **12** 112310
[24] Hoang G.T. *et al* 2004 *Phys. Rev. Lett.* **93** 135003
[25] Weisen H. *et al* 2006 *Plasma Phys. Control. Fusion* **47** A457
[26] Romanelli M. *et al* 2007 *Plasma Phys. Control. Fusion* **49** 935
[27] Willensdorfer M. *et al* 2013 *Nucl. Fusion* **53** 093020
[28] Callen J.D. *et al* 2010 *Nucl. Fusion* **50** 064004
[29] Groebner R.J. *et al* 2013 *Nucl. Fusion* **53** 093024
[30] Houlberg W.A. *et al* 1997 *Phys. Plasmas* **4** 3230
[31] Tala T. *et al* 2006 *Nuclear Fusion* **46** 548
[32] Howard N. *et al* 2014 *Phys. Plasmas* **21** 032308
[33] Artaud J.F. *et al* 2005 *Proc. 32nd EPS Conf. on Plasma Physics (Tarragona, Spain, 7 June–1 July 2005)* vol 29C (ECA) P-1.035 (http://epsppd.epfl.ch/Tarragona/pdf/P1_035.pdf)
[34] Angioni C. and Peeters A.G. 2006 *Phys. Rev. Lett.* **96** 095003
[35] Bourdelle C. *et al* 2005 *Plasma Phys. Control. Fusion* **47** A317
[36] Garbet X. *et al* 2003 *Phys. Rev. Lett.* **91** 035001
[37] Angioni C. *et al* 2003 *Phys. Rev. Lett.* **90** 205003
[38] Maslov M. *et al* 2009 *Nucl. Fusion* **49** 075037
[39] Weisen H. *et al* 2005 *Nucl. Fusion* **45** L1
[40] Angioni C. *et al* 2004 *Nucl. Fusion* **44** 827
[41] Lee G.S. *et al* 1986 *Phys. Fluids* B **29** 3291
[42] Romanelli F. *et al* 2014 *Proc. 25th IAEA FEC 2014 (Saint Petersburg, Russia, 13–18 October 2014)* (www-pub.iaea.org/iaeameetings/46091/25th-Fusion-Energy-Conference-FEC-2014)